

Sequential Covariance Fitting for InSAR Phase Linking

Dana EL HAJJAR, *Student Member, IEEE*, Guillaume GINOLHAC, *Senior Member, IEEE*,
Yajing YAN, *Member, IEEE*, and Mohammed Nabil EL KORSO

Abstract—Traditional Phase-Linking (PL) algorithms are known for their high cost, especially with the huge volume of Synthetic Aperture Radar (SAR) images generated by Sentinel-1 SAR missions. Recently, a COvariance Fitting Interferometric Phase Linking (COFI-PL) approach has been proposed, which can be seen as a generic framework for existing PL methods. Although this method is less computationally expensive than traditional PL approaches, COFI-PL exploits the entire covariance matrix, which poses a challenge with the increasing time series of SAR images. However, COFI-PL, like traditional PL approaches, cannot accommodate the efficient inclusion of newly acquired SAR images. This paper overcomes this drawback by introducing a sequential integration of a block of newly acquired SAR images. Specifically, we propose a method for effectively addressing optimization problems associated with phase-only complex vectors on the torus based on the Majorization-Minimization framework.

Index Terms—Interferometric Phase Linking, sequential, newly acquired SAR images, covariance fitting problem

NOTATIONS

Notations	Description
\circ	element-wise (Hadamard) product
\cdot^H	transposed and complex conjugated operator (Hermitian)
\cdot^T	transposed operator
\cdot	tilde accentuation representing the entire dataset
$\bar{\cdot}$	bar accentuation representing the new items
\cdot^*	complex conjugated operator
$Re(\cdot)$	complex number real component
$tr(\cdot)$	trace matrix operator
$\log(\cdot)$	logarithm operator
$\mathbb{E}(\cdot)$	first-order moment operator
$\ \cdot\ _F^2$	frobenius norm
$ \cdot $	modulus operator

I. INTRODUCTION

InSAR techniques have seen a great development and improvement with the immense number of available Synthetic Aperture Radar (SAR) images [1], thanks to ongoing remote sensing missions such as Sentinel-1, TerraSAR-X, etc. Interferometric Synthetic Aperture Radar (InSAR) is widely used to monitor land movements for various applications such as volcano monitoring, natural disaster damages, urban development. The first InSAR techniques involved using two SAR images acquired at two different dates (2-pass InSAR)

to estimate ground movements. However, when the dates are far apart, the coherence between the two images

ACRONYMS

CCG	Complex Circular Gaussian
COFI-PL	COvariance Fitting Interferometric Phase Linking
COMET	COvariance Matching Estimation Technique
DS	Distributed Scatterer
DSI	Distributed Scatterer Interferometry
EVD	EigenValue Decomposition
ILS	Integer Least Square
InSAR	Interferometric Synthetic Aperture Radar
KL	Kullback-Leibler
MLE	Maximum Likelihood Estimator
MLE-PL	Phase Linking based on Maximum Likelihood Estimation
MM	Majorization-Minimization
MSE	Mean Squared Error
MT-InSAR	Multi-Temporal Interferometric Synthetic Aperture Radar
PCA	Principal Component Analysis
PL	Phase-Linking
PO	Phase-Only Sample Covariance Matrix
PS	Permanent Scatterer
PSI	Permanent Scatterer Interferometry
RGD	Remannian Gradient Descent
SAR	Synthetic Aperture Radar
SBAS	Small BAseline Subset
SCM	Sample Covariance Matrix
S-COFI-PL	Sequential COvariance Fitting Interferometric Phase Linking
S-MLE-PL	Sequential Phase Linking based on Maximum Likelihood Estimation

weakens, resulting in a significant information loss. As a result, leveraging the vast availability of SAR images from various missions, time-series-based approaches have been proposed to exploit the temporal correlation among these images. This concept can be summarized as Multi-Temporal Interferometric Synthetic Aperture Radar (MT-InSAR). An essential family in MT-InSAR analysis is called Distributed Scatterer Interferometry (DSI) which exploits groups of homogeneous scatterers called Distributed Scatterer (DS). A famous approach in DSI, called Phase-Linking (PL) [2–6], consists to retrieve SAR image phases from the full SAR images time series. For an overview of existing PL algorithms, refer to [7, 8]. The general principle consists of two steps: first, estimating the Sample Covariance Matrix (SCM) and using its modulus as a plug-in of the unknown coherence matrix, and second, estimating the phases vector of SAR images. However, this plug-in is non optimal due to the fact that it does not represent the Maximum Likelihood Estimator (MLE) of the coherence matrix, since the modulus operator is not holomorphic. The second approach, introduced in [5, 6, 9], presents the true MLE of the coherence matrix jointly with the phases vector

D. EL HAJJAR is with LISTIC (EA3703), University Savoie Mont-Blanc, and with L2S, CentraleSupélec, University Paris-Saclay. G. GINOLHAC and Y. YAN are with LISTIC (EA3703), University Savoie Mont-Blanc. M.N. EL KORSO is with L2S, CentraleSupélec, University Paris-Saclay. The source code is available on GitHub at the following address: <https://github.com/DanaElhajjar/S-COFI-PL>

and will be referenced as MLE-PL, for Phase Linking based on Maximum Likelihood Estimation, in the remaining of the paper.

For both approaches, the process is based on the optimization of the negative log-likelihood function of the data following a zero mean Complex Circular Gaussian (CCG) distribution, which may not always fit the data. Studies such as [9, 10] have shown that SAR images are better modeled by a heavy-tailed distribution than a Gaussian distribution. Some works developed versions of the PL based on a Non-Gaussian distribution [9] which demonstrated an improvement in the results. These algorithms are computationally intensive as they rely on the full covariance matrix estimation and consist of an iterative algorithm with two steps [5, 9]: *i*) estimating the phases vector, with an iterative Majorization-Minimization (MM) algorithm, and *ii*) estimating the coherence matrix. These two steps are also part of an iterative algorithm called Block Coordinate Descent (BCD). Additionally, in the non-Gaussian case, the estimation of the covariance matrix is computationally intensive, as it involves Tyler-type estimators [9], for which the estimation process itself is recursive.

From above, it is clear that the estimation of the covariance matrix plays an important role. An alternative of the MLE approach was proposed in [11], called COvariance Matching Estimation Technique (COMET), often requiring less computational effort while maintaining similar asymptotic properties. They consist of a set of statistical methods used for parameter estimation by matching the empirical and theoretical covariance matrices. They gained attention in the signal processing field due to their efficiency in solving various estimation problems. Covariance fitting approach was used in InSAR in [12], namely COvariance Fitting Interferometric Phase Linking (COFI-PL). The main idea is to refine the structure of a covariance matrix estimator by minimizing a projection criterion. COFI-PL can be seen as a generalization of most of the existing PL problems [12] while maintaining a lower cost than traditional PL methods. The problem centers on two key components: the chosen method for covariance matrix estimation and the selected matrix distance. These factors can significantly influence the overall performance. Various covariance matrix plug-in can be used such as the SCM, the Phase-Only Sample Covariance Matrix (PO), Tyler estimator, etc. Additionally, regularization techniques can also be adopted. Although theoretically less effective, COFI-PL has demonstrated strong and promising results in practice with real-world data [12]. A key advantage of this approach is its robustness, which stems from to the choice of the covariance matrix plug-in.

However, when a new image or several new images are added, traditional methods become computationally intensive because they depend on the estimation of the full covariance matrix. This matrix increases with each new SAR image, necessitating a complete re-estimation every time a new image is introduced. As a result, traditional methods struggle to manage this growth, imposing significant constraints on real-time processing of SAR image time series. This often leads to inefficiencies and may fall short of operational requirements. To the best of our knowledge, only few studies addressed the

forementioned issue. Specifically, a sequential PL approach was proposed in [13], namely, Sequential Phase Linking based on Maximum Likelihood Estimation (S-MLE-PL), which incorporates each newly acquired SAR image with a much lower computational cost while keeping the same performances as MLE-PL. Despite the good performance of this approach and the reduction in computation time, it incorporates new SAR images one by one within a Gaussian model framework. A sequential approach, proposed in [14], is able to incorporate a bloc of new images. It is based on treating each mini-stack by applying the classic PL and then compressing it into a single virtual image through Principal Component Analysis (PCA). Each obtained virtual image is then connected to the next mini-stack. This method uses a partial coherence matrix, which can limit the amount of information available for analysis and reduce the accuracy of the estimates.

In this paper, we aim to develop a sequential approach that incorporates a stack of new SAR images, based on COFI-PL framework. We employ two matrix distances : Kullback-Leibler (KL) divergence and the Frobenius Norm, along with various covariance matrix estimators and potential regularization techniques. For each problem, we propose a MM algorithm to solve it. Results from simulations and real data demonstrate comparable outcomes to the benchmark, namely the offline approach COFI-PL.

In the following, a brief overview of COFI-PL is proposed in Section II. We present two matrix distances in Section II-B, different estimators of the covariance matrix in Section II-C and various ways to solve each problem in Section II-D. The description of our contribution starts at section III. Validation with experiments and real data are presented in Sections IV and V.

II. GENERIC COVARIANCE FITTING PROBLEM

Covariance fitting problems are prevalent across various domains, and several works have proposed different versions to address them [12, 15–20]. COMET consists of two steps: first, to estimate a plug-in of the covariance matrix, and second, to use a fitting criterion between the computed plug-in and a particular structure of the covariance matrix. In InSAR, [12, 21] proposed covariance fitting approaches to estimate phases while respecting the phase closure property.

A. InSAR model and optimization problem

For a given stack of l SAR images, we denote $\{\tilde{\mathbf{x}}^i\}_{i=1}^n$ the local homogeneous spatial neighborhood of size n for each pixel, where $\tilde{\mathbf{x}}^i \in \mathbb{C}^l$, for all $i \in \llbracket 1, n \rrbracket$. To ensure the temporal phase closure property, and based on standard physical properties [4], the covariance matrix of $\{\tilde{\mathbf{x}}^i\}_{i=1}^n$ can be formulated as

$$\tilde{\Sigma} = \tilde{\Psi} \odot \tilde{\mathbf{w}}_{\theta} \tilde{\mathbf{w}}_{\theta}^H \quad (1)$$

where $\tilde{\Psi}$ is the real core of the covariance matrix ($\tilde{\Psi} = |\tilde{\Sigma}|$), i.e. the coherence matrix scaled by the variances coefficients, $\tilde{\mathbf{w}}_{\theta}$ denotes the vector of the exponential of the complex phases.

In InSAR, the goal is to estimate the phases vector $\tilde{\mathbf{w}}_{\theta}$. Using the structure of the covariance matrix in equation (1), the

vector $\tilde{\mathbf{w}}_\theta$ can be estimated with COMET. At this point, the optimization problem is represented as

$$\begin{aligned} & \underset{\tilde{\mathbf{w}}_\theta}{\text{minimize}} && f_{\tilde{\Sigma}}^d(\tilde{\Sigma}, \tilde{\Psi} \circ \tilde{\mathbf{w}}_\theta \tilde{\mathbf{w}}_\theta^H) \\ & \text{subject to} && \theta_1 = 0 \\ & && \tilde{\mathbf{w}}_\theta \in \mathbb{T}_l \end{aligned} \quad (2)$$

with $\mathbb{T}_l = \{\tilde{\mathbf{w}}_\theta \in \mathbb{C}^l \mid |[\tilde{\mathbf{w}}_\theta]_i| = 1, \forall i \in [1, l]\}$. The objective function of the problem (2) is a matrix distance between the plug-in of the covariance matrix (possibly regularized) and its projection where the subscript $\tilde{\Sigma}$ consists of the covariance matrix plug-in, the superscript d denotes the chosen distance. Based on [12], we consider two distances, the Kullback-Leibler (KL) divergence and the Frobenius norm. For the plug-in, the classic SCM as well as a robust version will be used. For regularization, we consider the shrinking to identity and the tapering. The primary objective is to demonstrate the sequential adaptation of the approach rather than evaluating the efficiency of each distance and each estimator. The corresponding distances are presented in the following section.

B. Matrix distances

In this section, we introduce the KL divergence and the Frobenius norm.

1) Kullback-Leibler divergence

The KL divergence measures the similarity between two probability density functions. Between two centered Gaussian distributions, the KL divergence has the following form

$$\begin{aligned} KL(\mathcal{CN}(0, \Sigma_1) \parallel \mathcal{CN}(0, \Sigma_2)) \\ = \text{tr}(\Sigma_2^{-1} \Sigma_1) + \log(|\Sigma_2 \Sigma_1^{-1}|) - l \end{aligned} \quad (3)$$

In our context, Σ_1 represents the plug-in of the covariance matrix, and Σ_2 corresponds to the covariance matrix structure in equation (1), leading to the following structure of the objective function

$$f_{\tilde{\Sigma}}^{\text{KL}}(\tilde{\mathbf{w}}_\theta) = \tilde{\mathbf{w}}_\theta^H (\tilde{\Psi}^{-1} \circ \tilde{\Sigma}) \tilde{\mathbf{w}}_\theta \quad (4)$$

The KL divergence, shown in equation (4), between the Gaussian distribution with SCM as a plug-in for the covariance matrix and the Gaussian distribution with the structure of the covariance matrix in equation (1), corresponds to the objective function of the classic PL [4].

2) Frobenius norm

The Frobenius norm (also called Euclidean distance) of a matrix is defined as the sum of the absolute squares of its elements. The Frobenius norm between two symmetric matrices is defined as

$$d_F^2(\Sigma_1, \Sigma_2) = \|\Sigma_1 - \Sigma_2\|_F^2 \quad (5)$$

By setting $\Sigma_1 = \tilde{\Sigma}$ and $\Sigma_2 = \tilde{\Psi} \circ \tilde{\mathbf{w}}_\theta \tilde{\mathbf{w}}_\theta^H$, the simplified form of the corresponding objective function is obtained as

$$f_{\tilde{\Sigma}}^{\text{FN}}(\tilde{\mathbf{w}}_\theta) = -2\tilde{\mathbf{w}}_\theta^H (\tilde{\Psi} \circ \tilde{\Sigma}) \tilde{\mathbf{w}}_\theta \quad (6)$$

As it appears, the main interest between the two objective functions is the absence of the covariance matrix inversion in equation (6).

C. Covariance matrix plug-in

In this section, we present the various covariance matrix plug-in (Section II-C1) and the possible regularization (Section II-C2).

1) Unstructured covariance matrix

In this section, we present two estimators: the Sample Covariance Matrix (SCM) and the Phase-Only Sample Covariance Matrix (PO). In most PL approaches, the SCM is used and yields efficient results. In [12], the PO estimator was proposed and showed an improvement compared to other plug-in. In the remainder of the paper, the superscript index of a matrix represents the choice of the plug-in method (U : unconstrained, SK : shrinkage to identity regularization and BW : bandwidth (tapering regularization)).

a) Sample Covariance Matrix (SCM)

SCM is a common plug-in for the covariance matrix in InSAR processing [2, 4, 8, 22, 23]. This choice comes from the MLE of the covariance matrix $\tilde{\Sigma}$ according to a centered CCG model ($\tilde{\mathbf{x}} \sim \mathcal{CN}(0, \tilde{\Sigma})$)

$$\tilde{\Sigma}^U = \frac{1}{n} \sum_{i=1}^n \tilde{\mathbf{x}}^i \tilde{\mathbf{x}}^{iH} \quad (7)$$

SCM plug-in for the covariance matrix yields good results, however it is not robust when the data deviate from Gaussianity. SCM plug-in for the covariance matrix constitutes an efficient estimator when the data follows a Gaussian distribution. When the data deviate from Gaussianity or present outliers, a major deterioration in performances is observed [9, 12].

b) Phase-Only Sample Covariance Matrix (PO)

Let $\Phi_{\mathbb{T}} : x = r e^{i\theta} \rightarrow e^{i\theta}$ and $\tilde{\mathbf{y}} = \Phi_{\mathbb{T}}(\tilde{\mathbf{x}})$ represents the vector obtained by applying the transformation $\Phi_{\mathbb{T}}$ to the vector $\tilde{\mathbf{x}}$. The PO plug-in is defined as follow

$$\tilde{\Sigma}^U = \frac{1}{n} \sum_{i=1}^n \tilde{\mathbf{y}}^i \tilde{\mathbf{y}}^{iH} \quad (8)$$

The advantage of the corresponding estimator is the mitigation of amplitudes variations among SAR images [8], unlike the SCM. Additionally, it offers a balance between robustness and computation time, unlike the Tyler estimator, which is significantly more costly to compute.

2) Covariance matrix regularization

PL faces several challenges including the quality of the covariance matrix estimation. In fact, the accuracy of the covariance matrix estimation depends on the sample size n , which must be more than twice the length of the time series. For long time series, in situations such as $n \approx l$ or

$n < l$, the covariance matrix estimation is deemed inaccurate. Additionally, in such cases, the matrix inversion may also pose challenges due to the matrix being either ill-conditioned or singular. Moreover, matrix inversion is a required step in all the algorithms [4, 5, 9, 12]. A popular strategy to improve the covariance matrix estimation, is to use a regularization form [24–29]. The introduction of this regularization in Interferometric Phase Linking (IPL) was discussed in [30], and several works proposed such regularization [12, 21, 31–33]

a) Shrinkage to identity

As known, most covariance matrix estimators are unsatisfactory for large covariance estimation problems since they require huge sample support. In standard PL approaches, there is a significant chance of needing to invert a matrix such as SCM. This requires a large sample size to obtain an accurate estimation of the inversion. Additionally, the sample size increases with the length of the time series. The most common strategy for dealing with the problem of few samples is to shrink the estimator in question to a target matrix. An attractive case is to shrink the estimator to a scaled identity matrix [25, 30]. In other words, it is a combination between the covariance matrix estimator and the target matrix. The shrinkage parameter β has a closed form under an assumption of Gaussian model [27].

$$\tilde{\Sigma}^{SK} = \beta \tilde{\Sigma}^U + (1 - \beta) \frac{\text{tr}(\tilde{\Sigma}^U)}{l} \mathbf{I}_l \quad (9)$$

with $\beta \in [0, 1]$. Several combinations can be formed as in [27, 29, 34].

b) Covariance matrix tapering

InSAR approaches based on PL exploit all possible combinations between SAR images through the use of the covariance matrix. However, long SAR images time series suffer from target decorrelations as time progresses, resulting in near zero coherence among image pairs. The idea of the covariance matrix tapering regularization is to exclude pairs of images suffering from low coherence, which is done through the bandwidth b of the tapering matrix. Several techniques can be used to choose the value of b [29, 35, 36]. The interest of such regularization was discussed in [12, 21, 32, 33]. The covariance matrix tapering has the following form

$$[\tilde{\mathbf{W}}(b)]_{ij} = \begin{cases} 1 & \text{if } |i - j| \leq b \\ 0 & \text{otherwise} \end{cases} \quad (10)$$

Using (10), the covariance matrix tapering has the following form:

$$\tilde{\Sigma}^{BW} = \tilde{\mathbf{W}}(b) \circ \tilde{\Sigma}^U \quad (11)$$

A combination of shrinkage regularization and tapering was proposed in [29].

D. Optimization method

We propose a MM algorithm to solve the optimization problem in (2). We note that this problem can also be solved using Riemannian Gradient Descent (RGD), which can be advantageous for cost functions that cannot be expressed in a quadratic

form [12], making it unsuitable for the MM algorithm. The benefit of Riemannian optimization on the manifold lies in its ability to automatically compute the euclidean gradient of any cost function, facilitated by Python’s JAX package. However, this method requires identifying a hyper-parameter that will serve as the step size in the gradient descent. Each of these two methods has its advantages, but importantly, both ultimately lead to similar results [12], highlighting their effectiveness in solving the optimization problem. That said, the MM algorithm has the additional advantage of being computationally faster than RGD [12]. Given that we use the KL divergence and the Frobenius norm (with their ability to take a quadratic form), the MM algorithm is sufficient.

MM framework is composed of two main steps. The first step is called “Majorization”, where the objective is to find a surrogate function $g(\cdot | \mathbf{w}_\theta^{(t)})$ that majorizes the function $f(\mathbf{w}_\theta)$ and whose form depends on $\mathbf{w}^{(t)}$

$$f(\mathbf{w}_\theta) \leq g(\mathbf{w}_\theta | \mathbf{w}_\theta^{(t)}), \quad \forall \mathbf{w}_\theta \in \mathbb{T}_l \quad (12)$$

In other words, $g(\mathbf{w}_\theta | \mathbf{w}_\theta^{(t)})$ is tangent to $f(\mathbf{w}_\theta)$ at the point $\mathbf{w}_\theta = \mathbf{w}_\theta^{(t)}$. For the KL divergence and the Frobenius norm, the following Lemmas are used respectively to find the corresponding surrogate.

Lemma 1 *The convex quadratic form*

$$f : \mathbf{w}_\theta \longrightarrow \mathbf{w}_\theta^H \mathbf{H} \mathbf{w}_\theta \quad (13)$$

is majored on \mathbb{T}_l by :

$$g(\mathbf{w}_\theta | \mathbf{w}_\theta^{(t)}) = 2\text{Re} \left(\mathbf{w}_\theta^H (\mathbf{H} - \lambda_{max}^H \mathbf{I}) \mathbf{w}_\theta^{(t)} \right) + const \quad (14)$$

with equality at point $\mathbf{w}_\theta^{(t)}$. λ_{max}^H corresponds to the largest eigenvalue of \mathbf{H} [12].

Lemma 2 *The concave quadratic form*

$$f : \mathbf{w}_\theta \longrightarrow -\mathbf{w}_\theta^H \mathbf{H} \mathbf{w}_\theta \quad (15)$$

is majored, with equality at point $\mathbf{w}^{(t)}$ [12], by :

$$g(\mathbf{w}_\theta | \mathbf{w}_\theta^{(t)}) = -2\text{Re}(\mathbf{w}^H \mathbf{H} \mathbf{w}_\theta^{(t)}) \quad (16)$$

The second step, “Minimization” includes obtaining the next iterate of the corresponding parameter by minimizing the obtained function $g(\cdot | \mathbf{w}_\theta^{(t)})$ rather than the actual function $f(\mathbf{w}_\theta)$

$$\mathbf{w}_\theta^{(t+1)} = \underset{\mathbf{w}_\theta \in \mathbb{T}_l}{\text{argmin}} g(\mathbf{w}_\theta | \mathbf{w}_\theta^{(t)}) \quad (17)$$

For both matrix distances, Lemma 3 is used to minimize the surrogate function.

Lemma 3 *The solution of the following minimization problem*

$$\underset{\bar{\mathbf{w}}_\theta \in \mathbb{T}_k}{\text{minimize}} \quad -\text{Re}(\bar{\mathbf{w}}_\theta^H \tilde{\mathbf{w}}_\theta^{(t)}) \quad (18)$$

is obtained as $\bar{\mathbf{w}}_\theta^* = \Phi_{\mathbb{T}}(\tilde{\mathbf{w}}_\theta^{(t)})$ with $\Phi_{\mathbb{T}} : x = r e^{i\theta} \rightarrow e^{i\theta}$ [12]

The main key to a successful MM algorithm consists in the step of constructing the function $g(\cdot | \mathbf{w}_\theta^{(t)})$ [37]. The advantage

of this framework remains in the low computational cost of the obtained optimization problem. MM algorithms have been already used in InSAR [5, 9]. Further details on MM algorithms are provided in [37–41].

To summarize this section, we defined the optimization problem for estimating the complete phase time series, as well as the matrix distances and covariance matrix plug-in. In the following section, we will present the sequential formulation of the COFI-PL problem.

III. SEQUENTIAL FORMULATION OF COVARIANCE FITTING

A. Data model and optimization problem

We consider a stack of $l = p + k$ SAR images (p represents the length of the SAR images time series of the past and k the number of newly acquired SAR images). $\{\tilde{\mathbf{x}}^i\}_{i=1}^n$ denotes the local homogeneous spatial neighborhood of size n for a given pixel, where $\tilde{\mathbf{x}}^i \in \mathbb{C}^l$, for all $i \in [1, n]$, i.e.,

$$\tilde{\mathbf{x}}^i = \underbrace{[x_1^i, \dots, x_p^i]}_{\mathbf{x}^i}, \underbrace{[x_{p+1}^i, \dots, x_l^i]}_{\bar{\mathbf{x}}^i} \in \mathbb{C}^l \quad (19)$$

where $\mathbf{x}^i \in \mathbb{C}^p$ denotes the multivariate pixel of the previous data, and $\bar{\mathbf{x}}^i \in \mathbb{C}^k$ for the new ones (Fig. 1). Each pixel of the local patch is assumed to be distributed as a zero mean Complex Circular Gaussian (CCG) [42], i.e., $\tilde{\mathbf{x}} \sim \mathcal{CN}(0, \tilde{\Sigma})$.

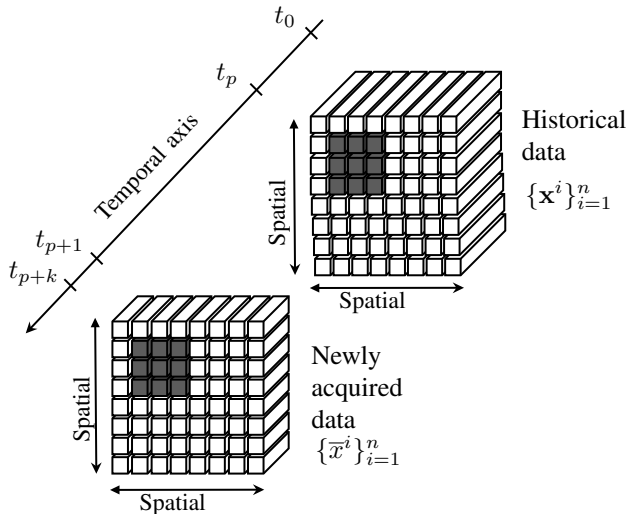


Fig. 1: SAR data representation including both previous and recently obtained block of images. The local neighborhood of size n is denoted by gray pixels (sliding window).

The vector of phases of the entire set of images can be expressed as a block structure as follow

$$\tilde{\mathbf{w}}_\theta = \begin{pmatrix} \mathbf{w}_\theta \\ \bar{\mathbf{w}}_\theta \end{pmatrix} \quad (20)$$

where \mathbf{w}_θ denotes the exponential phases vector for the previous data, and $\bar{\mathbf{w}}_\theta$ denotes the exponential phase vector for the new ones. The covariance matrix of the entire set of images can be expressed as the following block structure

$$\tilde{\Sigma} = \begin{pmatrix} \Sigma_p & (\Sigma_{pn})^H \\ \Sigma_{pn} & \Sigma_n \end{pmatrix} \quad (21)$$

where Σ_p represents the covariance and coherence matrices, respectively, of the block of past images, both of which have dimensions (p, p) . Meanwhile, Σ_{pn} denotes the covariance and coherence, respectively, between the past images and the new ones with dimensions (k, p) . Additionally, Σ_n corresponds to the covariance and coherence matrices of the block of new images, with dimensions (k, k) .

In the remainder of the paper, the subscript index of a matrix indicates the block type (p : past images, pn : interaction between past and new images and n : new images). For each plug-in, we present its detailed block structure as follow

1) Unstructured plug-in: SCM or PO

The covariance matrix, whether it is SCM (equation (7)) or PO (equation (8)), can be represented in the following block structure

$$\tilde{\Sigma}^U = \begin{pmatrix} \Sigma_p^U & (\Sigma_{pn}^U)^H \\ \Sigma_{pn}^U & \Sigma_n^U \end{pmatrix} \quad (22)$$

2) Shrinkage to identity

The block structure of the shrinkage to identity regularization of a plug-in of the covariance matrix in equation (9) can be represented as follow

$$\begin{aligned} \tilde{\Sigma}^{SK} &= \beta \tilde{\Sigma}^U + (1 - \beta) \frac{\text{tr}(\tilde{\Sigma}^U)}{l} \mathbf{I}_l \\ &= \begin{pmatrix} \beta \Sigma_p^U + (1 - \beta) \frac{\text{tr}(\tilde{\Sigma}^U)}{l} \mathbf{I}_p & \beta (\Sigma_{pn}^U)^H \\ \beta \Sigma_{pn}^U & \beta \Sigma_n^U + (1 - \beta) \frac{\text{tr}(\tilde{\Sigma}^U)}{l} \mathbf{I}_k \end{pmatrix} \\ &= \begin{pmatrix} \Sigma_p^{SK} & (\Sigma_{pn}^{SK})^H \\ \Sigma_{pn}^{SK} & \Sigma_n^{SK} \end{pmatrix} \end{aligned} \quad (23)$$

given that the estimator $\tilde{\Sigma}^U$ can be either the SCM or PO as in equation (22).

3) Covariance matrix tapering

The tapering matrix with bandwidth b in equation (10) can have the following block structure

$$\tilde{\mathbf{W}}(b) = \begin{pmatrix} \mathbf{W}_p & (\mathbf{W}_{pn})^T \\ \mathbf{W}_{pn} & \mathbf{W}_n \end{pmatrix} \quad (24)$$

Using the structure in equation (21), the tapered covariance matrix can be partitioned into a block structure comprising three distinct components: one representing the past $\mathbf{W}_p \circ \Sigma_p$, one corresponding to the new data $\mathbf{W}_n \circ \Sigma_n$, and a third capturing the interaction between the two $\mathbf{W}_{pn} \circ \Sigma_{pn}$ as follow

$$\begin{aligned} \tilde{\Sigma}^{BW} &= \tilde{\mathbf{W}}(b) \circ \tilde{\Sigma}^U \\ &= \begin{pmatrix} \mathbf{W}_p \circ \Sigma_p^U & (\mathbf{W}_{pn})^T \circ (\Sigma_{pn}^U)^H \\ \mathbf{W}_{pn} \circ \Sigma_{pn}^U & \mathbf{W}_n \circ \Sigma_n^U \end{pmatrix} \\ &= \begin{pmatrix} \Sigma_p^{BW} & (\Sigma_{pn}^{BW})^H \\ \Sigma_{pn}^{BW} & \Sigma_n^{BW} \end{pmatrix} \end{aligned} \quad (25)$$

The optimization problem is formulated as follow

$$\begin{aligned} &\underset{\tilde{\mathbf{w}}_\theta}{\text{minimize}} && f_\Sigma^d(\tilde{\Sigma}, \tilde{\Psi} \circ \tilde{\mathbf{w}}_\theta \tilde{\mathbf{w}}_\theta^H) \\ &\text{subject to} && \theta_1 = 0 \\ &&& \tilde{\mathbf{w}}_\theta \in \mathbb{T}_k \end{aligned} \quad (26)$$

where $\bar{\mathbf{w}}_\theta$ is defined in equation (20). $f_{\tilde{\Sigma}}^d(\tilde{\Sigma}, \tilde{\Psi} \circ \tilde{\mathbf{w}}_\theta \tilde{\mathbf{w}}_\theta^H)$ is the cost function of the COMET problem and depends on $\bar{\mathbf{w}}_\theta$. For each distance, a generic form is provided in the sections (III-B, III-C).

	unconstrained plug-in (section III-A1)	shrinkage to identity (section III-A2)	tapering regularization (section III-A3)
	SCM \ PO	SK-SCM \ SK-PO	BW-SCM \ BW-PO
Σ_p	Σ_p^U	Σ_p^{SK}	Σ_p^{BW}
Σ_{pn}	Σ_{pn}^U	Σ_{pn}^{SK}	Σ_{pn}^{BW}
Σ_n	Σ_n^U	Σ_n^{SK}	Σ_n^{BW}

TABLE I: Σ_p , Σ_{pn} and Σ_n values depending on the choice of the covariance matrix plug-in.

B. Kullback-Leibler divergence

In this section, we provide a general form of the cost function for the KL divergence presented in Proposition 1, which can be applied and modified according to the choice of the covariance matrix plug-in in Table I

Proposition 1 Generic cost function for KL divergence

Regardless the choice of the covariance matrix plug-in, the cost function for the KL divergence has the following form

$$\begin{aligned}
 f_{\tilde{\Sigma}}^{KL}(\bar{\mathbf{w}}_\theta) &= \mathbf{w}_\theta^H (\mathbf{F}^{-1} \circ \Sigma_p) \mathbf{w}_\theta \\
 &+ \mathbf{w}_\theta^H ((\mathbf{A})^T \circ (\Sigma_{pn})^H) \bar{\mathbf{w}}_\theta \\
 &+ \bar{\mathbf{w}}_\theta^H (\mathbf{A} \circ \Sigma_{pn}) \mathbf{w}_\theta \\
 &+ \bar{\mathbf{w}}_\theta^H \mathbf{M} \bar{\mathbf{w}}_\theta
 \end{aligned} \tag{27}$$

where

- $\mathbf{F} = |\Sigma_p| - (|\Sigma_{pn}|)^T |\Sigma_n|^{-1} |\Sigma_{pn}|$
- $\mathbf{D} = |\Sigma_n| - |\Sigma_{pn}| |\Sigma_p|^{-1} (|\Sigma_{pn}|)^T$
- $\mathbf{A} = -\mathbf{D}^{-1} |\Sigma_{pn}| |\Sigma_p|^{-1}$
- $\mathbf{M} = \mathbf{D}^{-1} \circ \Sigma_n$

and Σ_p , Σ_{pn} and Σ_n depend on the choice of the covariance matrix plug-in Table I.

PROOF in Appendix A-A.

For each case of the generic cost function for the KL divergence in equation (27) and after a few calculations steps, it corresponds to the convex quadratic form in Lemma 1. Similar to the cost function, we present a generic form for the surrogate function that majorizes the corresponding cost function in equation (27).

Proposition 2 Surrogate function for KL divergence

Using Lemma 1, we majorize the cost function in equation (27) by the following surrogate function

$$\begin{aligned}
 g(\bar{\mathbf{w}}_\theta | \bar{\mathbf{w}}_\theta^{(t)}) &= -\text{Re} \left(\bar{\mathbf{w}}_\theta^H 2 [(-\mathbf{A}) \circ \Sigma_{pn}] \mathbf{w}_\theta \right. \\
 &\quad \left. - [\mathbf{M} - \lambda_{\max}^{\mathbf{M}} \mathbf{I}_k] \bar{\mathbf{w}}_\theta^{(t)} \right)
 \end{aligned} \tag{28}$$

where $\lambda_{\max}^{\mathbf{M}}$ corresponds to the largest eigenvalue of \mathbf{M} and Σ_p , Σ_{pn} and Σ_n are presented in Table I.

PROOF in Appendix B-A

The equivalent optimization to the problem (26) is

$$\underset{\bar{\mathbf{w}}_\theta \in \mathbb{T}_k}{\text{minimize}} \quad g(\bar{\mathbf{w}}_\theta | \bar{\mathbf{w}}_\theta^{(t)}) \tag{29}$$

and is solved using Lemma 3. The MM algorithm is presented in the box Algorithm 1.

Algorithm 1 MM for KL divergence

- 1: **Input:** $\tilde{\Sigma} \in \mathbb{C}^l$, $\mathbf{w}_\theta^{(0)} \in \mathbb{T}_l$
- 2: Compute : $\mathbf{M} = (\mathbf{D}^{-1} \circ \Sigma_n)$ and $\lambda_{\max}^{\mathbf{M}}$
- 3: Compute $\mathbf{N} = 2 [(-\mathbf{A}) \circ \Sigma_{pn}] \mathbf{w}_\theta$
- 4: **repeat**
- 5: Compute $\ddot{\mathbf{w}}_\theta^{(t)} = \mathbf{N} - (\mathbf{M} - \lambda_{\max}^{\mathbf{M}} \mathbf{I}) \bar{\mathbf{w}}_\theta^{(t)}$
- 6: Update of $\bar{\mathbf{w}}_\theta^{(t)} = \Phi_{\mathbb{T}}\{\ddot{\mathbf{w}}_\theta^{(t)}\}$
- 7: $t = t + 1$
- 8: **until** convergence
- 9: **Output:** $\hat{\mathbf{w}}_\theta = \mathbf{w}_{\text{end}} \in \mathbb{T}_k$

C. Frobenius norm

Similar to the KL divergence, this section is also divided into two parts: the first part addresses the cost functions, followed by the second part that provide the optimization algorithm. We provide a generic form of the cost function for the Frobenius norm that can be applied to any covariance matrix plug-in.

Proposition 3 Generic cost function for the Frobenius norm

The cost function for the Frobenius norm is represented in the following form

$$\begin{aligned}
 f_{\tilde{\Sigma}}^{LS}(\bar{\mathbf{w}}_\theta) &= -2\mathbf{w}_\theta^H (|\Sigma_p| \circ \Sigma_p) \mathbf{w}_\theta \\
 &\quad - 2\mathbf{w}_\theta^H (|\Sigma_{pn}|)^T \circ (\Sigma_{pn})^H \bar{\mathbf{w}}_\theta \\
 &\quad - 2\bar{\mathbf{w}}_\theta^H (|\Sigma_{pn}| \circ \Sigma_{pn}) \mathbf{w}_\theta \\
 &\quad - 2\bar{\mathbf{w}}_\theta^H (|\Sigma_n| \circ \Sigma_n) \bar{\mathbf{w}}_\theta
 \end{aligned} \tag{30}$$

where Σ_p , Σ_{pn} and Σ_n are presented in Table I.

PROOF in Appendix A-B

As for the KL divergence, the Frobenius norm has a quadratic form that enables the use of the MM algorithm. Using Lemma 2, the cost function in equation (30) can be majorized by a function $g(\bar{\mathbf{w}}_\theta | \bar{\mathbf{w}}_\theta^{(t)})$ which will be provided in what follows, where we present a generic form that can be applied to any covariance matrix plug-in.

Proposition 4 Surrogate function for Frobenius norm

The cost function can be majorized on \mathbb{T}_k by the following surrogate function

$$\begin{aligned}
 g(\bar{\mathbf{w}}_\theta | \bar{\mathbf{w}}_\theta^{(t)}) &= -\text{Re} \left(\bar{\mathbf{w}}_\theta^H \cdot 4 [(|\Sigma_{pn}| \circ \Sigma_{pn}) \mathbf{w}_\theta \right. \\
 &\quad \left. + (|\Sigma_n| \circ \Sigma_n) \bar{\mathbf{w}}_\theta^{(t)} \right]
 \end{aligned} \tag{31}$$

where Σ_{pn} and Σ_n are presented in Table I.

PROOF in Appendix B-B

Then the minimization problem can be solved using Lemma 3. The MM algorithm is presented in the box Algorithm 2.

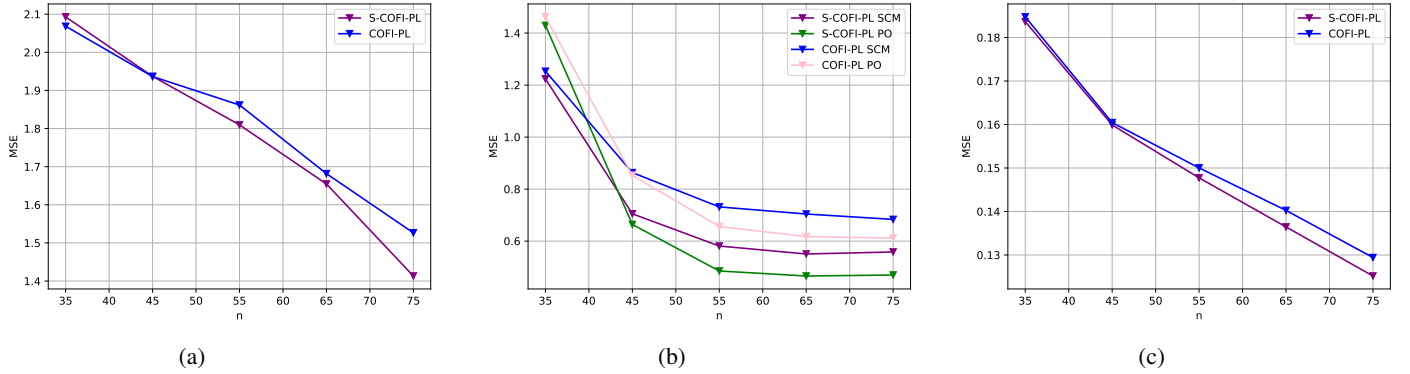


Fig. 2: MSE of phase difference estimation between the 1st and 40th (last) dates for $l = 40$ with respect to increasing sample size (n) with KL divergence. 1st column: SCM using gaussian simulated data, 2nd column: SCM and PO using non-gaussian simulated data, 3rd column: SK-PO to identity with $\beta = 0.9$ using gaussian simulated data.

Algorithm 2 MM for Frobenius norm

- 1: **Input:** $\tilde{\Sigma} \in \mathbb{C}^l$, $\mathbf{w}_\theta^{(1)} \in \mathbb{T}_l$
 - 2: Compute $\mathbf{M} = |\Sigma_{pn}| \circ \Sigma_{pn}$
 - 3: Compute $\mathbf{N} = |\Sigma_n| \circ \Sigma_n$
 - 4: **repeat**
 - 5: Compute $\tilde{\mathbf{w}}_\theta^{(t)} = \mathbf{M} + \mathbf{N}\tilde{\mathbf{w}}_\theta^{(t)}$
 - 6: Update of $\tilde{\mathbf{w}}_\theta^{(t)} = \Phi_{\mathbb{T}}\{\tilde{\mathbf{w}}_\theta^{(t)}\}$
 - 7: $t = t + 1$
 - 8: **until** convergence
 - 9: **Output:** $\hat{\mathbf{w}}_\theta = \tilde{\mathbf{w}}_\theta^{(\text{end})} \in \mathbb{T}_k$
-

D. Complexity comparison study

PL methods are considered to be costly, especially as they handle matrices whose size depends on the length of the time series of images used. For the KL divergence, the computational complexity depends on matrix inversion and Singular Value Decomposition (SVD) decomposition. In S-COFI-PL, these operations are performed on (k, k) matrices, while in COFI-PL, they are performed on $(p + k, p + k)$ matrices. For the Frobenius norm, where matrix inversion is no longer needed, the complexity is based on matrix multiplications. In S-COFI-PL, this involves matrices of size (k, k) and (k, p) , whereas in the COFI-PL method, it involves matrices of size $(p + k, p + k)$. The complexity of the presented methods are reported in Table II.

Method	Complexity	
S-MLE-PL [13]	$O((l-1)^3)$	
Sequential Estimator [14]	$O(5(k^3 + m^3) + (k^2 + m^2))$	
S-COFI-PL	KL divergence	$O(2k^3 + k^2 + kp)$
	Frobenius norm	$O(kp + k^2)$
COFI-PL [43]	KL divergence	$O(2l^3 + l^2)$
	Frobenius norm	$O(l^2)$

TABLE II: Complexity comparison for S-MLE-PL [13], Sequential Estimator [14] where m represents the number of compressed images, S-COFI-PL and COFI-PL for both KL divergence and the Frobenius norm.

IV. NUMERICAL EXPERIMENTS

We simulate a time series of size $l = p + k = 40$ images, where $p = 35$ and $k = 5$. The real core of the

covariance matrix $\tilde{\Psi}$ is simulated as a Toeplitz matrix i.e., $[\tilde{\Psi}]_{ij} = \rho^{|i-j|}$ with a coefficient correlation $\rho = 0.98$. Phases differences vary linearly between 0 and 2 rad, i.e., $\Delta_{i,i-1} = \theta_i - \theta_{i-1} = 2/l$ rad. The covariance matrix is then obtained according to equation (1). We consider two scenarios and we simulate n independent and identically distributed (i.i.d) samples according to

- Gaussian distribution assumption: $\tilde{\mathbf{x}}^i \sim \mathcal{N}(0, \tilde{\Sigma})$
- Non Gaussian distribution assumption: $\tilde{\mathbf{x}}^i \sim \mathcal{N}(0, \tau_i \tilde{\Sigma})$, where each τ_i is sampled following a Gamma distribution $\tau \sim \Gamma(\nu, \frac{1}{\nu})$ with $\nu = 1$.

We compare the results of our approach with the offline COFI-PL approach [12]. Several matrix distances and covariance matrix plug-in are used and presented. Mean Squared Error (MSE) are computed using 1000 Monte Carlo trials.

Fig. 2 provides the MSE of phase estimate when the sample size n increases. Fig. 2 (a) shows a comparison of phase estimates with SCM as a plug-in for the covariance matrix between the offline COFI-PL approach and the sequential S-COFI-PL approach. The phase difference estimations from these 2 approaches yield similar accuracy. Fig. 2 (b) can be analysed in 2 different setups, comparing the offline and sequential approaches, and second, comparing the plug-in SCM with the PO. For this case, we used the data simulated according to a Non Gaussian distribution. It is known that, in the context of covariance matrix estimation, robust estimators behave equivalently to estimators based on a Gaussian model assumption when the data follow a Gaussian distribution [44, 45]. However, when the data follow a Non Gaussian distribution, the performance improvement is significant [9], as it is showed in Fig. 2 (b). Fig. 2 (c) shows a comparison between the sequential and offline processing with the shrinkage to identity regularization for the covariance matrix plug-in. Both approaches yields similar results.

Fig. 3 represents the MSE of phase estimates when n increases using the Frobenius norm. Fig. 3 (a) shows that taking the SCM as a plug-in yields similar results for the sequential and offline approaches. As in the case of the KL divergence, PO yields better results than the SCM when applied to Non Gaussian data (Fig. 3 (b)). Fig. 3 (c) shows similar performances between the S-COFI-PL and COFI-PL when

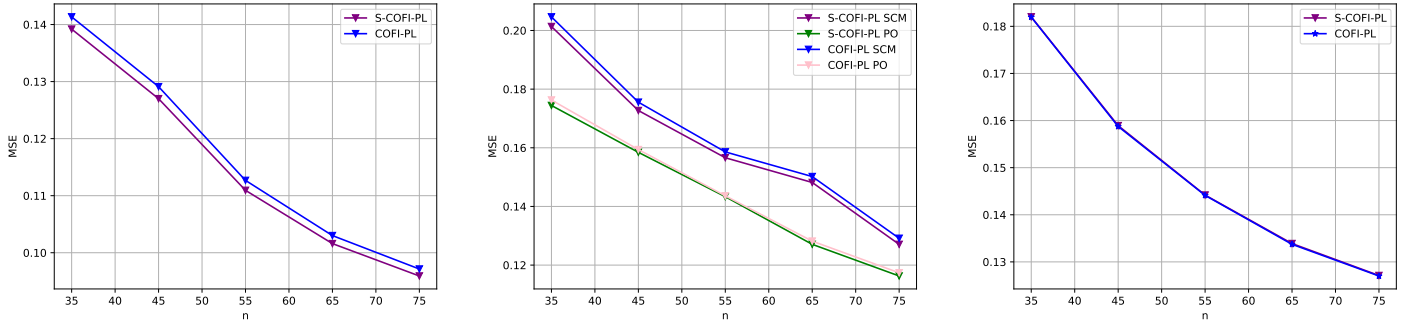


Fig. 3: MSE of phase difference estimation between the 1st and 40th (last) dates for $l = 40$ with respect to increasing sample size (n) with Frobenius norm. 1st column: SCM using gaussian simulated data, 2nd column: SCM and PO using non-gaussian simulated data, 3rd column: BW-PO with $b = 9$ using gaussian simulated data.

taking a tapering regularization for the PO.

As shown, the sequential approach S-COFI-PL yields similar results to the offline method COFI-PL [12]. Nonetheless, it is interesting to study the scenario of integrating sequentially several blocks of new SAR images, in order to analyze the error propagation in the estimated phase. Let’s consider a scenario of having a total of t SAR images. We consider the following decomposition for the sequential treatment :

- p SAR images represent the first block, which will be used to apply the COFI-PL
- k SAR images represent the second block, which will be used to apply the S-COFI-PL approach along with the first block
- m SAR images represent the third block. The estimation of the m phases will be examined in several ways. First, using the offline COFI-PL approach where $t = p+k+m$ SAR images are used directly. Second, the m phases are estimated according to the $l = p + k$ past images which can be approached in two way: the offline method and the concatenation of p phases computed offline with k phases calculated sequentially.

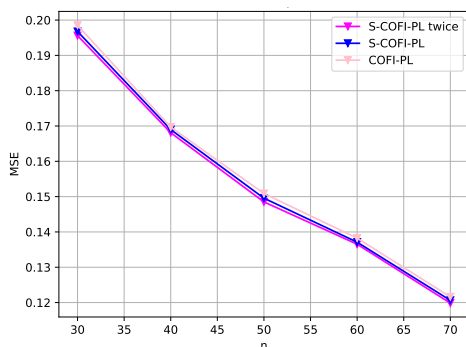


Fig. 4: MSE on \bar{w}_θ with increasing n , $t = 40$, $\rho = 0.98$ using 1000 Monte Carlo trials.

Fig. 4 represents MSE variations on \bar{w}_θ with an increase in sample size n . For the simulations, we consider a scenario of a total of $t = 40$ images, divided into 3 blocks. The first block is of size $p = 30$, the second block is of size $k = 5$, and the third block is of size $m = 5$. The coherence matrix is simulated

as a Toeplitz matrix with a coefficient correlation $\rho = 0.98$. PO is used as a plug-in for the covariance matrix with the Frobenius norm as a matrix distance. The application once of the sequential method, S-COFI-PL, yields results similar to the offline method, COFI-PL. The successive integration of multiple blocks of new SAR images, taking into account the results of the sequential method progressively, shows similar performances, in terms of MSE, as the offline approach COFI-PL and the sequential approach S-COFI-PL applied once.

V. REAL WORLD STUDY

A. Study area and dataset

Ranking among the five largest cities in the world, Mexico city has a population exceeding 20 million habitants. It covers 2000 km², 2300 m above sea level. Mexico city went through rapid urbanization, which led to a significant increase in demand for water. The primary water supply comes from aquifers, leading to subsidence and deformation across the city. Mexico city consists of an interesting case study for many multi-temporal InSAR approaches. We used a data set of 40 SAR images over Mexico city, acquired between 14 August 2019 and 18 December 2021, every 12 days. Pre-processing treatment was done via SNAP software [46] where all images are co-registered with reference to the first date 14 August 2019. In order to relate to the parameters in the simulations, $p = 35$, $k = 5$, the sample size is set to $n = 64$ (i.e sliding window of size 8×8 pixels).

For this study, we focus on the comparison of the results of S-COFI-PL with the offline approach COFI-PL [12, 43], and the sequential approaches proposed in [13, 14].

B. Qualitative assessment of the estimated phase

In Fig. 5 and Fig. 6, we show only the estimation of the interferogram with the longest temporal baseline of 857 days, to emphasize performance in relation to temporal decorrelation. We provide results for various covariance matrix estimations, however our objective is to compare the outcomes of the sequential and offline approaches, regardless the chosen plug-in for the covariance matrix. Detailed comparison is made in

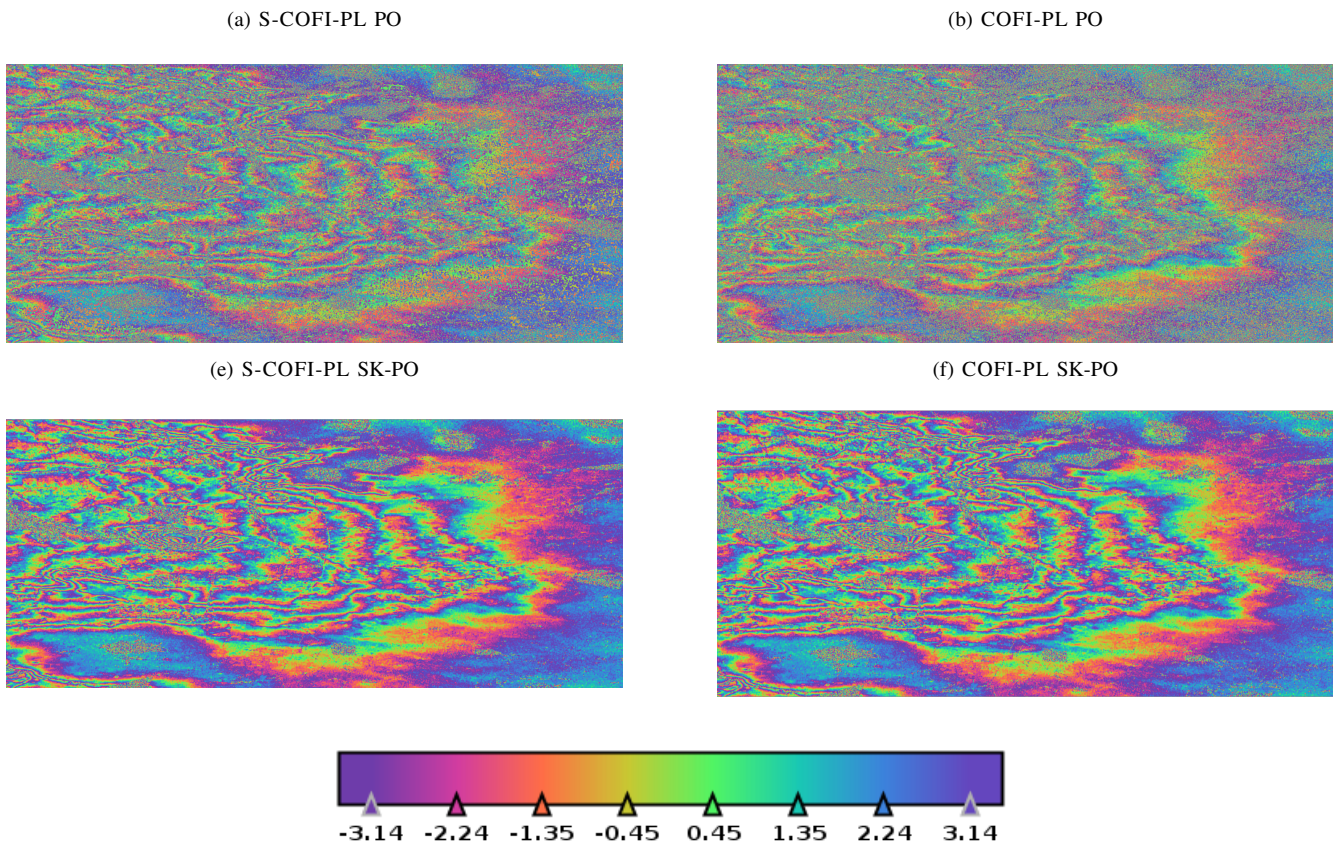


Fig. 5: The longest temporal baseline interferograms estimated by S-COFI-PL (1st column) and COFI-PL [12] (2nd column) with various plug-in estimators for the covariance matrix and KL divergence. 1st row: PO, 2nd row: SK-PO

[12] between the different matrix distances that can be used, as well as the different covariance matrix plug-in.

Fig. 5 presents the results for the KL divergence. As highlighted in [43], the choice of the plug-in estimator significantly impacts the quality of the resulting interferogram (see the comparison in rows in Fig. 5). The PO plug-in shows superior performance in the sequential approach S-COFI-PL (Fig. 5 (a)) compared to the offline method COFI-PL (Fig. 5 (b)). The KL divergence function requires matrix inversion, which becomes increasingly complex as the matrix size grows. This issue is less problematic in the sequential processing, as the inversion is applied to smaller matrices, thereby enhancing the results compared to the offline processing. Additionally, after closer inspection, the shrinking to identity regularization (SK-PO) demonstrates superior performance in the sequential processing S-COFI-PL compared to the offline COFI-PL (Fig. 5 (c) and (d)). The performances of S-COFI-PL and COFI-PL, in Fig. 6, are similar. A comparison of the interferograms in the two columns reveals comparable quality and noise levels throughout the scene. Additionally, a comparison of the different plug-ins is illustrated in Fig. 6 (a), (b), with the PO plug-in, Fig. 6 (c), (d), with the shrinking of the PO plug-in, and Fig. 6 (e), (f) with the tapering regularization of the PO plug-in. Upon closer examination, as mentioned in [43], regularization, particularly tapering, yields superior results.

Fig. 7 represents the results of the sequential approaches in the state-of-the-art [13, 14]. The Sequential Estimator [14]

shows performance comparable to that of shrinking the PO to the identity using the KL divergence, though the latter remains slightly noisier. This result is not surprising, as the sequential estimator can be viewed as a low-rank approximation. In [12], it was shown that the low-rank structure of the covariance matrix yields results similar to those obtained with shrinkage regularization to the identity. However, the sequential estimator appears to be outperformed by the PO, SK-PO, and BW-PO estimators using the Frobenius norm, which are less noisy compared to the sequential estimator. The S-MLE-PL proposed in [13] is expected to yield similar results to S-COFI-PL with SCM as a plug-in with the KL divergence.

C. Quantitative assessment of the estimated phase

In Table III, we show values of several quantitative criteria such as Root Mean Squared Error (RMSE), Spatial Correlation Coefficient (SCC), Universal image Quality Index (UQI), Structural SIMilarity index (SSIM) and the colinearity criterion [47]. The colinearity criterion evaluates whether the results are noisy and allows spatial comparison of the phase with its surroundings. A value closer to 1 indicates better results. We select the results of the offline approach COFI-PL with the Frobenius norm and the BW-PO regularization as our baseline, which outperforms state-of-art approaches as demonstrated in [12]. The first axis of comparison is between the offline and sequential processing. For the KL divergence, comparable results are observed between the two processing

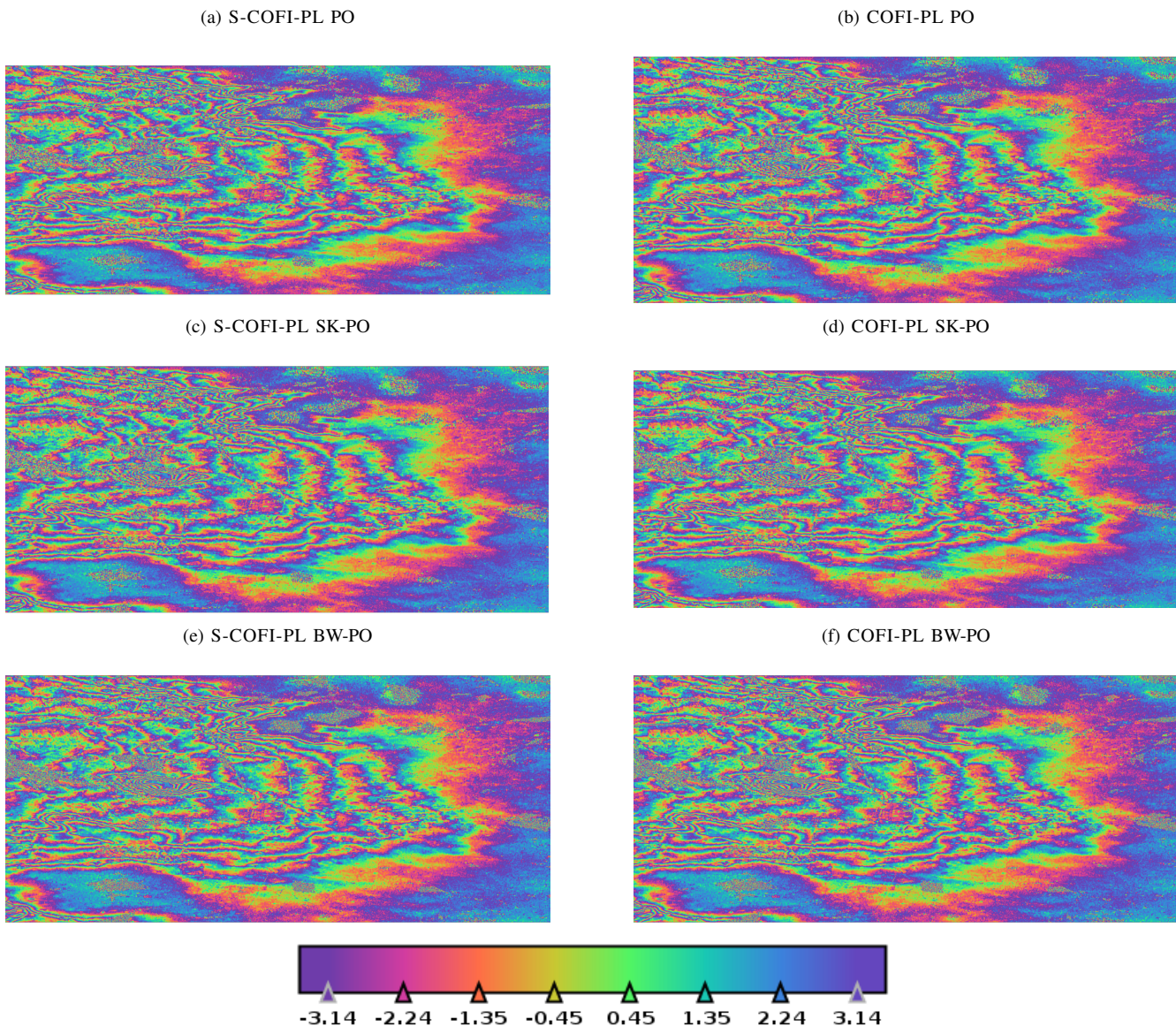


Fig. 6: The longest temporal baseline interferograms estimated by S-COFI-PL (1st column) and COFI-PL [12] (2nd column) with various plug-in estimators for the covariance matrix with Frobenius norm. 1st row: SCM, 2nd row: SK-PO, 3rd row: BW-PO

approaches, where in most cases, S-COFI-PL outperforms COFI-PL. As shown in Fig. 5 ((a) and (b)), the sequential processing with PO yields better results than the offline processing.

For the Frobenius norm, similar values are observed across all indicators for both sequential and offline processing with each plug-in. The colinearity of outputs is also similar in both sequential and offline approaches, consequently achieving values greater than 0.85. Compared to state-of-the-art sequential methods, S-COFI-PL with the Frobenius norm delivers superior performance irrespective of the chosen plug-in. For the KL divergence, S-COFI-PL achieves better results with the shrinking-to-identity regularization. For other metrics, the sequential estimator [14] generally performs better. With the sequential S-MLE-PL method [13], S-COFI-PL using the Frobenius norm yields better results across all plug-ins. For S-COFI-PL with the KL divergence, similar performance to

BW-SCM is observed, which is better than SCM and BW-PO. Otherwise, with other plug-ins and regularizations, S-COFI-PL demonstrates superior results.

D. Computation time comparison

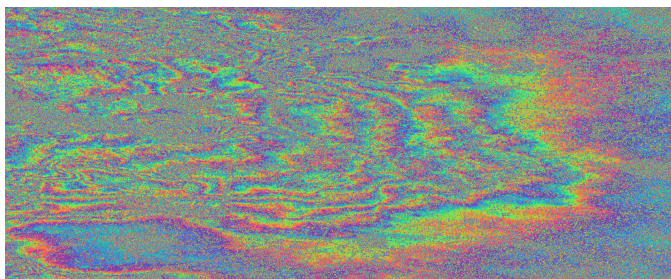
Method		Computation time
S-MLE-PL [13]		2.18h
Sequential Estimator [14]		0.6h
S-COFI-PL	KL divergence	0.44h
	Frobenius norm	0.37h
COFI-PL [43]	KL divergence	0.52h
	Frobenius norm	0.43h

TABLE IV: Computation time comparison for S-MLE-PL [13], Sequential Estimator [14], S-COFI-PL and COFI-PL for both KL divergence and the Frobenius norm

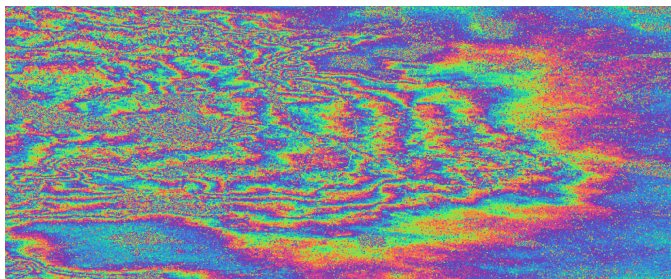
As shown in the complexity comparison (section III-D), the proposed approach is less costly than the sequential ap-

		RMSE	SCC	UQI	SSIM	colinearity [47]
KL divergence	S-COFI-PL SCM	2.63	1.00	0.05	0.0003	0.21
	COFI-PL SCM	2.51	0.93	0.07	0.001	0.24
	S-COFI-PL PO	2.01	0.55	0.36	0.11	0.55
	COFI-PL PO	2.11	0.63	0.27	0.06	0.42
	S-COFI-PL SK-SCM	2.03	0.55	0.39	0.13	0.61
	COFI-PL SK-SCM	2.03	0.56	0.38	0.12	0.60
	S-COFI-PL SK-PO	1.35	0.23	0.73	0.58	0.90
	COFI-PL SK-PO	1.40	0.25	0.70	0.53	0.87
	S-COFI-PL BW-SCM	2.63	0.98	0.08	0.001	0.31
	COFI-PL BW-SCM	2.63	1.01	0.09	0.002	0.32
Frobenius norm	S-COFI-PL SCM	1.80	0.42	0.56	0.28	0.87
	COFI-PL SCM	1.80	0.43	0.56	0.28	0.87
	S-COFI-PL PO	1.31	0.22	0.74	0.61	0.94
	COFI-PL PO	1.32	0.23	0.74	0.60	0.94
	S-COFI-PL SK-SCM	1.80	0.42	0.56	0.28	0.87
	COFI-PL SK-SCM	1.80	0.43	0.56	0.28	0.87
	S-COFI-PL SK-PO	1.31	0.22	0.74	0.61	0.94
	COFI-PL SK-PO	1.32	0.23	0.74	0.60	0.94
	S-COFI-PL BW-SCM	1.76	0.41	0.57	0.30	0.85
	COFI-PL BW-SCM	1.76	0.41	0.57	0.30	0.85
Sequential Estimator [14]		1.82	0.44	0.53	0.24	0.81
S-MLE-PL [13]		2.34	0.74	0.18	0.01	0.33

TABLE III: Quantitative evaluation and comparison of different approaches



(a) S-MLE-PL



(b) Sequential Estimator

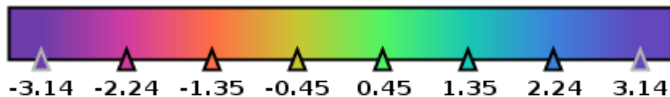


Fig. 7: The longest temporal baseline interferogram estimated by (a) S-MLE-PL [13] and (b) Sequential Estimator [14] with a stack of size $k = 5$.

proaches proposed in the state-of-the-art as well as the offline approaches. In this section, we compare the computation time of each approach applied in Mexico City data set of 40 images of size (3638, 16709) pixels. We use a machine with a 95-

core CPU running at 2.2 GHz and 125 G of RAM with calculations executed in parallel across the CPUs. We show the computation time of each approach in the table IV.

For a comparison between the offline processing and our approach, the latter is faster than the COFI-PL [43] offline algorithm for KL (17%) and Frobenius norm (13%). In comparison with the sequential approaches in the state of the art, our approach is faster than the S-MLE-PL method [13] (78% and 83% for KL and Frobenius, respectively), as well as the sequential estimator [14] (63% and 68% for KL and Frobenius, respectively).

ACKNOWLEDGMENT

This work is funded by the ANR REPED-SARIX project (ANR-21-CE23-0012-01) of the French national Agency of research.

VI. CONCLUSION

In this paper, we propose a novel sequential approach based on covariance fitting interferometric PL. The proposed framework accommodates the KL divergence and the Frobenius norm as well as various plug-in for the covariance matrix estimation, which, through different regularization methods, ensure the robustness of the approach. We provide a MM algorithm to solve the different optimization problems. Numerical experiments and real-world study shows the efficiency of the proposed approach in terms of performances and computation time.

REFERENCES

[1] B. Osmanoğlu, F. Sunar, S. Wdowinski, and E. Cabral-Cano, “Time series analysis of InSAR data: Methods and trends,” *ISPRS Journal of Photogrammetry and Remote Sensing*, vol. 115, pp. 90–102, 2016.

- [2] A. Ferretti, A. Fumagalli, F. Novali, C. Prati, F. Rocca, and A. Rucci, "A new algorithm for processing interferometric data-stacks: SqueeSAR," *IEEE transactions on geoscience and remote sensing*, vol. 49, no. 9, pp. 3460–3470, 2011.
- [3] H. Ansari, F. De Zan, and R. Bamler, "Efficient phase estimation for interferogram stacks," *IEEE Transactions on Geoscience and Remote Sensing*, vol. 56, no. 7, pp. 4109–4125, 2018.
- [4] A. Guarnieri and S. Tebaldini, "On the exploitation of target statistics for SAR interferometry applications," *IEEE Transactions on Geoscience and Remote Sensing*, vol. 46, no. 11, pp. 3436–3443, 2008.
- [5] P. Vu, F. Brigui, A. Breloy, Y. Yan, and G. Ginolhac, "A new phase linking algorithm for multi-temporal InSAR based on the Maximum Likelihood Estimator," in *IGARSS 2022 IEEE International Geoscience and Remote Sensing Symposium*. IEEE, 2022, pp. 76–79.
- [6] C. Wang, X. Wang, Y. Xu, Bochen Zhang, M. Jiang, S. Xiong, Q. Zhang, W. Li, and Q. Li, "A New Likelihood Function for Consistent Phase Series Estimation in Distributed Scatterer Interferometry," *IEEE Transactions on Geoscience and Remote Sensing*, vol. 60, pp. 1–14, 2022.
- [7] D. Minh and S. Tebaldini, "Interferometric Phase Linking: Algorithm, application, and perspective," *IEEE Geoscience and Remote Sensing Magazine*, vol. 11, no. 3, pp. 46–62, 2023.
- [8] N. Cao, H. Lee, and H. Jung, "Mathematical framework for phase-triangulation algorithms in distributed-scatterer interferometry," *IEEE Geoscience and Remote Sensing Letters*, vol. 12, no. 9, pp. 1838–1842, 2015.
- [9] P. Vu, A. Breloy, F. Brigui, Y. Yan, and G. Ginolhac, "Robust Phase Linking in InSAR," *IEEE Transactions on Geoscience and Remote Sensing*, vol. 61, pp. 1–11, 2023.
- [10] A. Mian, G. Ginolhac, J-P. Ovarlez, and A.M. Atto, "New robust statistics for change detection in time series of multivariate SAR images," *IEEE Transactions on Signal Processing*, vol. 67, no. 2, pp. 520–534, 2018.
- [11] B. Ottersten, P. Stoica, and R. Roy, "Covariance matching estimation techniques for array signal processing applications," *Digital Signal Processing*, vol. 8, no. 3, pp. 185–210, 1998.
- [12] P. Vu, A. Breloy, F. Brigui, Y. Yan, and G. Ginolhac, "Covariance Fitting Interferometric Phase Linking: Modular Framework and Optimization Algorithms," *arXiv preprint arXiv:2403.08646*, 2024.
- [13] D. El Hajjar, Y. Yan, G. Ginolhac, and M.N. El Korso, "Sequential phase linking: progressive integration of SAR images for operational phase estimation," in *IGARSS IEEE International Geoscience and Remote Sensing Symposium*. IEEE, 2024.
- [14] H. Ansari, F. De Zan, and R. Bamler, "Sequential Estimator: Toward efficient InSAR time series analysis," *IEEE Transactions on Geoscience and Remote Sensing*, vol. 55, no. 10, pp. 5637–5652, 2017.
- [15] B. Mériaux, C. Ren, M.N. El Korso, A. Breloy, P. Forster, and J-P. Ovarlez, "On the recursions of Robust COMET algorithm for convexly structured shape matrix," in *2019 27th European Signal Processing Conference (EU-SIPCO)*. IEEE, 2019, pp. 1–5.
- [16] B. Mériaux, C. Ren, M.N. El Korso, A. Breloy, and P. Forster, "Robust estimation of structured scatter matrices in (MIS) matched models," *Signal Processing*, vol. 165, pp. 163–174, 2019.
- [17] W. Hu, J. Xue, and N. Zheng, "PSF Estimation via Covariance Matching," in *ICASSP*, 2010, pp. 1354–1357.
- [18] K. Werner, M. Jansson, and P. Stoica, "On estimation of covariance matrices with Kronecker product structure," *IEEE Transactions on Signal Processing*, vol. 56, no. 2, pp. 478–491, 2008.
- [19] B. Mériaux, C. Ren, M.N. El Korso, A. Breloy, and P. Forster, "Robust-COMET for covariance estimation in convex structures: algorithm and statistical properties," in *2017 IEEE 7th International Workshop on Computational Advances in Multi-Sensor Adaptive Processing (CAMSAP)*. IEEE, 2017, pp. 1–5.
- [20] B. Mériaux, C. Ren, A. Breloy, M.N. El Korso, and P. Forster, "Matched and mismatched estimation of kronecker product of linearly structured scatter matrices under elliptical distributions," *IEEE Transactions on Signal Processing*, vol. 69, pp. 603–616, 2020.
- [21] Y. Bai, J. Kang, X. Ding, A. Zhang, Z. Zhang, and N. Yokoya, "LaMIE: Large-Dimensional Multipass InSAR Phase Estimation for Distributed Scatterers," *IEEE Transactions on Geoscience and Remote Sensing*, vol. 61, pp. 1–15, 2023.
- [22] A. Ferretti, C. Prati, and F. Rocca, "Permanent Scatterers in SAR Interferometry," *IEEE Transactions on geoscience and remote sensing*, vol. 39, no. 1, pp. 8–20, 2001.
- [23] G. Fornaro, S. Verde, D. Reale, and A. Pauciuolo, "CAESAR: An approach based on covariance matrix decomposition to improve multibaseline–multitemporal interferometric SAR processing," *IEEE Transactions on Geoscience and Remote Sensing*, vol. 53, no. 4, pp. 2050–2065, 2014.
- [24] O. Ledoit and M. Wolf, "A well-conditioned estimator for large-dimensional covariance matrices," *Journal of multivariate analysis*, vol. 88, no. 2, pp. 365–411, 2004.
- [25] Y. Chen, A. Wiesel, Y.C. Eldar, and A.O. Hero, "Shrinkage algorithms for MMSE covariance estimation," *IEEE transactions on signal processing*, vol. 58, no. 10, pp. 5016–5029, 2010.
- [26] A. Rucci, S. Tebaldini, and F. Rocca, "Skp-shrinkage estimator for SAR multi-baselines applications," in *2010 IEEE Radar Conference*. IEEE, 2010, pp. 701–706.
- [27] X. Chen, Z.J. Wang, and M.J. McKeown, "Shrinkage-to-tapering estimation of large covariance matrices," *IEEE Transactions on Signal Processing*, vol. 60, no. 11, pp. 5640–5656, 2012.
- [28] F. Pascal, Y. Chitour, and Y. Quek, "Generalized robust shrinkage estimator and its application to STAP detection problem," *IEEE Transactions on Signal Processing*, vol. 62, no. 21, pp. 5640–5651, 2014.

- [29] E. Ollila and A. Breloy, “Regularized tapered sample covariance matrix,” *IEEE Transactions on Signal Processing*, vol. 70, pp. 2306–2320, 2022.
- [30] M. Even and K. Schulz, “InSAR deformation analysis with distributed scatterers: A review complemented by new advances,” *Remote Sensing*, vol. 10, no. 5, pp. 744, 2018.
- [31] S. Zwieback, “Cheap, valid regularizers for improved interferometric phase linking,” *IEEE Geoscience and Remote Sensing Letters*, vol. 19, pp. 1–4, 2022.
- [32] H. Liang, L. Zhang, X. Li, and J. Wu, “Coherence bias mitigation through regularized tapered coherence matrix for phase linking in decorrelated environments,” *ISPRS Journal of Photogrammetry and Remote Sensing*, vol. 215, pp. 369–382, 2024.
- [33] C. Zhao, H. Yu, and Y. Wang, “A Regularized Coherence Matrix Estimation Method for Phase Linking in Distributed Scatterer Interferometry,” in *IGARSS IEEE International Geoscience and Remote Sensing Symposium*. IEEE, 2024, pp. 2403–2406.
- [34] Y. Chen, A. Wiesel, and A.O. Hero, “Robust shrinkage estimation of high-dimensional covariance matrices,” *IEEE Transactions on Signal Processing*, vol. 59, no. 9, pp. 4097–4107, 2011.
- [35] P.J. Bickel and E. Levina, “Regularized Estimation of Large Covariance Matrices,” *The Annals of Statistics*, vol. 36, no. 1, pp. 199–227, 2008.
- [36] P.J. Bickel and E. Levina, “Covariance Regularization by Thresholding,” *The Annals of Statistics*, vol. 36, no. 6, pp. 2577–2604, 2008.
- [37] Y. Sun, P. Babu, and D.P. Palomar, “Majorization-Minimization algorithms in signal processing, communications, and machine learning,” *IEEE Transactions on Signal Processing*, vol. 65, no. 3, pp. 794–816, 2016.
- [38] D.R. Hunter and K. Lange, “A tutorial on MM algorithms,” *The American Statistician*, vol. 58, no. 1, pp. 30–37, 2004.
- [39] M. Razaviyayn, M. Hong, and Z.Q. Luo, “A unified convergence analysis of block successive minimization methods for nonsmooth optimization,” *SIAM Journal on Optimization*, vol. 23, no. 2, pp. 1126–1153, 2013.
- [40] M. Soltanalian and P. Stoica, “Designing unimodular codes via quadratic optimization,” *IEEE Transactions on Signal Processing*, vol. 62, no. 5, pp. 1221–1234, 2014.
- [41] A. Breloy, S. Kumar, Y. Sun, and D.P. Palomar, “Majorization-minimization on the Stiefel manifold with application to robust sparse PCA,” *IEEE Transactions on Signal Processing*, vol. 69, pp. 1507–1520, 2021.
- [42] R. Bamler and P. Hartl, “Synthetic Aperture Radar Interferometry,” *Inverse problems*, vol. 14, no. 4, pp. R1, 1998.
- [43] P.V.H. Vu, A. Breloy, F. Brigui, Y. Yan, and G. Ginolhac, “Covariance fitting based InSAR Phase Linking,” in *IGARSS IEEE International Geoscience and Remote Sensing Symposium*. IEEE, 2023, pp. 8234–8237.
- [44] F. Pascal, J.P. Barbot, H. Harari-Kermadec, R. Suyama, and P. Larzabal, “An empirical likelihood method for data aided channel identification in unknown noise field,” in *2008 16th European Signal Processing Conference*. IEEE, 2008, pp. 1–5.
- [45] H. Harari-Kermadec and F. Pascal, “On the use of empirical likelihood for non-gaussian clutter covariance matrix estimation,” in *2008 IEEE Radar Conference*. IEEE, 2008, pp. 1–6.
- [46] European Space Agency (ESA), “SNAP,” <https://step.esa.int/main/toolboxes/snap>.
- [47] Béatrice Pinel-Puysségur, Rémi Michel, and Jean-Philippe Avouac, “Multi-link InSAR time series: Enhancement of a wrapped interferometric database,” *IEEE Journal of Selected Topics in Applied Earth Observations and Remote Sensing*, vol. 5, no. 3, pp. 784–794, 2012.
- [48] K.B. Petersen, M.S. Pedersen, et al., “The matrix cookbook,” *Technical University of Denmark*, vol. 7, no. 15, pp. 510, 2008.

APPENDIX A

CALCULATION DETAILS OF THE COST FUNCTIONS

We recall the block structure of the covariance matrix

$$\tilde{\Sigma} = \begin{pmatrix} \Sigma_p & (\Sigma_{pn})^H \\ \Sigma_{pn} & \Sigma_n \end{pmatrix}$$

where the different notations are provided in Table V.

	unconstrained plug-in (section III-A1)	shrinkage to identity regularization (section III-A2)	tapering regularization (section III-A3)
	SCM \ PO	SK-SCM \ SK-PO	BW-SCM \ BW-PO
Σ_p	Σ_p^U	Σ_p^{SK}	Σ_p^{BW}
Σ_{pn}	Σ_{pn}^U	Σ_{pn}^{SK}	Σ_{pn}^{BW}
Σ_n	Σ_n^U	Σ_n^{SK}	Σ_n^{BW}

TABLE V: Σ_p , Σ_{pn} and Σ_n values depending on the choice of the covariance matrix plug-in.

In this appendix, we provide the various calculation steps to derive the generic form of the cost function for the KL divergence and the Frobenius norm respectively.

A. Kullback-Leibler divergence

By designating

- $\mathbf{F} = |\Sigma_p| - (|\Sigma_{pn}|)^T |\Sigma_n|^{-1} |\Sigma_{pn}|$
- $\mathbf{D} = |\Sigma_n| - |\Sigma_{pn}| |\Sigma_p|^{-1} (|\Sigma_{pn}|)^T$
- $\mathbf{A} = -\mathbf{D}^{-1} |\Sigma_{pn}| |\Sigma_p|^{-1}$
- $\mathbf{M} = \mathbf{D}^{-1} \circ \Sigma_n$

the inverse of a block structured matrix [48] has the following form

$$\tilde{\Psi}^{-1} = \begin{pmatrix} \mathbf{F}^{-1} & (\mathbf{A})^T \\ \mathbf{A} & \mathbf{D}^{-1} \end{pmatrix}$$

The cost function in equation (27) for the KL divergence is obtained as follow

$$\begin{aligned} f_{\tilde{\Sigma}}^{\text{KL}}(\tilde{\mathbf{w}}_\theta) &= \tilde{\mathbf{w}}_\theta^H (\tilde{\Psi}^{-1} \circ \tilde{\Sigma}) \tilde{\mathbf{w}}_\theta \\ &= \begin{pmatrix} \mathbf{w}_\theta \\ \bar{\mathbf{w}}_\theta \end{pmatrix}^H \left(\begin{pmatrix} \mathbf{F}^{-1} & (\mathbf{A})^T \\ \mathbf{A} & \mathbf{D}^{-1} \end{pmatrix} \circ \begin{pmatrix} \Sigma_p & (\Sigma_{pn})^H \\ \Sigma_{pn} & \Sigma_n \end{pmatrix} \right) \begin{pmatrix} \mathbf{w}_\theta \\ \bar{\mathbf{w}}_\theta \end{pmatrix} \\ &= \begin{pmatrix} \mathbf{w}_\theta \\ \bar{\mathbf{w}}_\theta \end{pmatrix}^H \begin{pmatrix} \mathbf{F}^{-1} \circ \Sigma_p & (\mathbf{A})^T \circ (\Sigma_{pn})^H \\ \mathbf{A} \circ \Sigma_{pn} & \mathbf{M} \end{pmatrix} \begin{pmatrix} \mathbf{w}_\theta \\ \bar{\mathbf{w}}_\theta \end{pmatrix} \\ &= \begin{pmatrix} \mathbf{w}_\theta \\ \bar{\mathbf{w}}_\theta \end{pmatrix}^H \begin{pmatrix} (\mathbf{F}^{-1} \circ \Sigma_p) \mathbf{w}_\theta + ((\mathbf{A})^T \circ (\Sigma_{pn})^H) \bar{\mathbf{w}}_\theta \\ (\mathbf{A} \circ \Sigma_{pn}) \mathbf{w}_\theta + \mathbf{M} \bar{\mathbf{w}}_\theta \end{pmatrix} \\ &= \mathbf{w}_\theta^H (\mathbf{F}^{-1} \circ \Sigma_p) \mathbf{w}_\theta + \mathbf{w}_\theta^H ((\mathbf{A})^T \circ (\Sigma_{pn})^H) \bar{\mathbf{w}}_\theta \\ &\quad + \bar{\mathbf{w}}_\theta^H (\mathbf{A} \circ \Sigma_{pn}) \mathbf{w}_\theta + \bar{\mathbf{w}}_\theta^H \mathbf{M} \bar{\mathbf{w}}_\theta \end{aligned}$$

B. Frobenius norm

The generic cost function in equation (30) for the Frobenius norm is obtained as follow

$$\begin{aligned} f_{\tilde{\Sigma}}^{\text{FN}}(\tilde{\mathbf{w}}_\theta) &= -2\tilde{\mathbf{w}}_\theta^H (\tilde{\Psi} \circ \tilde{\Sigma}) \tilde{\mathbf{w}}_\theta \\ &= -2 \begin{pmatrix} \mathbf{w}_\theta \\ \bar{\mathbf{w}}_\theta \end{pmatrix}^H \left(\begin{pmatrix} |\Sigma_p| & (|\Sigma_{pn}|)^T \\ |\Sigma_{pn}| & |\Sigma_n| \end{pmatrix} \circ \begin{pmatrix} \Sigma_p & (\Sigma_{pn})^H \\ \Sigma_{pn} & \Sigma_n \end{pmatrix} \right) \begin{pmatrix} \mathbf{w}_\theta \\ \bar{\mathbf{w}}_\theta \end{pmatrix} \\ &= -2 \begin{pmatrix} \mathbf{w}_\theta \\ \bar{\mathbf{w}}_\theta \end{pmatrix}^H \begin{pmatrix} (|\Sigma_p| \circ \Sigma_p) \mathbf{w}_\theta + (|\Sigma_{pn}|)^T \circ (\Sigma_{pn})^H \bar{\mathbf{w}}_\theta \\ (|\Sigma_{pn}| \circ \Sigma_{pn}) \mathbf{w}_\theta + (|\Sigma_n| \circ \Sigma_n) \bar{\mathbf{w}}_\theta \end{pmatrix} \\ &= -2\mathbf{w}_\theta^H (|\Sigma_p| \circ \Sigma_p) \mathbf{w}_\theta \\ &\quad - 2\mathbf{w}_\theta^H (|\Sigma_{pn}|)^T \circ (\Sigma_{pn})^H \bar{\mathbf{w}}_\theta \\ &\quad - 2\bar{\mathbf{w}}_\theta^H (|\Sigma_{pn}| \circ \Sigma_{pn}) \mathbf{w}_\theta \\ &\quad - 2\bar{\mathbf{w}}_\theta^H (|\Sigma_n| \circ \Sigma_n) \bar{\mathbf{w}}_\theta \end{aligned}$$

APPENDIX B

CALCULATIONS DETAILS FOR THE MM ALGORITHM

In this appendix, we present the steps to derive the surrogate function for each of the distances, the KL divergence and the Frobenius norm respectively.

A. Kullback-Leibler divergence

The cost function in equation (27) can be reformulated as follow

$$\begin{aligned} f_{\tilde{\Sigma}}^{\text{KL}}(\tilde{\mathbf{w}}_\theta) &= \mathbf{w}_\theta^H (\mathbf{F}^{-1} \circ \Sigma_p) \mathbf{w}_\theta \\ &\quad + \mathbf{w}_\theta^H ((-|\Sigma_p|^{-1} (|\Sigma_{pn}|)^T \mathbf{D}^{-1}) \circ (\Sigma_{pn})^H) \bar{\mathbf{w}}_\theta \\ &\quad + \bar{\mathbf{w}}_\theta^H ((-\mathbf{D}^{-1} |\Sigma_{pn}| |\Sigma_p|^{-1}) \circ \Sigma_{pn}) \mathbf{w}_\theta \\ &\quad + \bar{\mathbf{w}}_\theta^H \mathbf{M} \bar{\mathbf{w}}_\theta \\ &\propto (\bar{\mathbf{w}}_\theta^H ((-\mathbf{D}^{-1} |\Sigma_{pn}| |\Sigma_p|^{-1}) \circ \Sigma_{pn}) \mathbf{w}_\theta)^H \\ &\quad + \bar{\mathbf{w}}_\theta^H ((-\mathbf{D}^{-1} |\Sigma_{pn}| |\Sigma_p|^{-1}) \circ \Sigma_{pn}) \mathbf{w}_\theta \\ &\quad + \bar{\mathbf{w}}_\theta^H \mathbf{M} \bar{\mathbf{w}}_\theta \\ &\propto 2\text{Re}(\bar{\mathbf{w}}_\theta^H ((-\mathbf{D}^{-1} |\Sigma_{pn}| |\Sigma_p|^{-1}) \circ \Sigma_{pn}) \mathbf{w}_\theta) \\ &\quad + \bar{\mathbf{w}}_\theta^H \mathbf{M} \bar{\mathbf{w}}_\theta \end{aligned}$$

Using Lemma 1, the above cost function can be majorized by the following expression

$$\begin{aligned} f_{\tilde{\Sigma}}^{\text{KL}}(\tilde{\mathbf{w}}_\theta) &\leq 2\text{Re}(\bar{\mathbf{w}}_\theta^H ((-\mathbf{D}^{-1} |\Sigma_{pn}| |\Sigma_p|^{-1}) \circ \Sigma_{pn}) \mathbf{w}_\theta) \\ &\quad + 2\text{Re}(\bar{\mathbf{w}}_\theta^H [\mathbf{M} - \lambda_{\max}^{\mathbf{M}} \mathbf{I}_k] \bar{\mathbf{w}}_\theta^{(t)}) \\ &= \text{Re}(2\bar{\mathbf{w}}_\theta^H ((-\mathbf{D}^{-1} |\Sigma_{pn}| |\Sigma_p|^{-1}) \circ \Sigma_{pn}) \mathbf{w}_\theta) \\ &\quad + 2\bar{\mathbf{w}}_\theta^H [\mathbf{M} - \lambda_{\max}^{\mathbf{M}} \mathbf{I}_k] \bar{\mathbf{w}}_\theta^{(t)}) \\ &= -\text{Re}(\bar{\mathbf{w}}_\theta^H 2 [((\mathbf{D}^{-1} |\Sigma_{pn}| |\Sigma_p|^{-1}) \circ \Sigma_{pn}) \mathbf{w}_\theta \\ &\quad - [\mathbf{M} - \lambda_{\max}^{\mathbf{M}} \mathbf{I}_k] \bar{\mathbf{w}}_\theta^{(t)})]) \end{aligned}$$

B. Frobenius norm

The cost function in equation (30) can be written as follow

$$\begin{aligned}
f_{\tilde{\Sigma}}^{\text{FN}}(\tilde{\mathbf{w}}_{\theta}) &= -2\mathbf{w}_{\theta}^H (|\Sigma_p| \circ \Sigma_p) \mathbf{w}_{\theta} \\
&\quad - 2\mathbf{w}_{\theta}^H (|\Sigma_{pn}|^T \circ (\Sigma_{pn})^H) \tilde{\mathbf{w}}_{\theta} \\
&\quad - 2\tilde{\mathbf{w}}_{\theta}^H (|\Sigma_{pn}| \circ \Sigma_{pn}) \mathbf{w}_{\theta} \\
&\quad - 2\tilde{\mathbf{w}}_{\theta}^H (|\Sigma_n| \circ \Sigma_n) \tilde{\mathbf{w}}_{\theta} \\
&\propto -2(\tilde{\mathbf{w}}_{\theta}^H (|\Sigma_{pn}| \circ \Sigma_{pn}) \mathbf{w}_{\theta})^H \\
&\quad - 2\tilde{\mathbf{w}}_{\theta}^H (|\Sigma_{pn}| \circ \Sigma_{pn}) \mathbf{w}_{\theta} \\
&\quad - 2\tilde{\mathbf{w}}_{\theta}^H (|\Sigma_n| \circ \Sigma_n) \tilde{\mathbf{w}}_{\theta} \\
&\propto -4\text{Re}(\tilde{\mathbf{w}}_{\theta}^H (|\Sigma_{pn}| \circ \Sigma_{pn}) \mathbf{w}_{\theta}) \\
&\quad - 2\tilde{\mathbf{w}}_{\theta}^H (|\Sigma_n| \circ \Sigma_n) \tilde{\mathbf{w}}_{\theta}
\end{aligned}$$

Using Lemma 2, the cost function can be majorized by the following expression

$$\begin{aligned}
f_{\tilde{\Sigma}}^{\text{FN}}(\tilde{\mathbf{w}}_{\theta}) &\leq -4\text{Re}(\tilde{\mathbf{w}}_{\theta}^H (|\Sigma_{pn}| \circ \Sigma_{pn}) \mathbf{w}_{\theta}) \\
&\quad - 4\text{Re}(\tilde{\mathbf{w}}_{\theta}^H (|\Sigma_n| \circ \Sigma_n) \tilde{\mathbf{w}}_{\theta}^{(t)}) \\
&= -4\text{Re}(\tilde{\mathbf{w}}_{\theta}^H (|\Sigma_{pn}| \circ \Sigma_{pn}) \mathbf{w}_{\theta} \\
&\quad + \tilde{\mathbf{w}}_{\theta}^H (|\Sigma_n| \circ \Sigma_n) \tilde{\mathbf{w}}_{\theta}^{(t)}) \\
&= -4\text{Re}(\tilde{\mathbf{w}}_{\theta}^H [(|\Sigma_{pn}| \circ \Sigma_{pn}) \mathbf{w}_{\theta} \\
&\quad + (|\Sigma_n| \circ \Sigma_n) \tilde{\mathbf{w}}_{\theta}^{(t)}]) \\
&= -\text{Re}(\tilde{\mathbf{w}}_{\theta}^H 4 [(|\Sigma_{pn}| \circ \Sigma_{pn}) \mathbf{w}_{\theta} \\
&\quad + (|\Sigma_n| \circ \Sigma_n) \tilde{\mathbf{w}}_{\theta}^{(t)}])
\end{aligned}$$